Arabian Journal for Science and Engineering (2020) 45:7397–7408
https://doi.org/10.1007/s13369-020-04544-0

RESEARCH ARTICLE-CHEMICAL ENGINEERING

Synthesis, Characterization and Dye Adsorption Performance of Strontium Ferrite decorated Bentonite-CoNiAl Magnetic Composite

Khalid H. A. Elkhider[1] · Ihsanullah Ihsanullah[2] · Mukarram Zubair[3] · Mohammad Saood Manzar[3] · Nuhu Dalhat Mu'azu[3] · Mamdouh A. Al-Harthi[1,4]

Received: 6 January 2020 / Accepted: 16 April 2020 / Published online: 2 May 2020

Abstract
In this study, a new magnetic adsorbent, strontium ferrite-bentonite-CoNiAl composite (SF-B-CoNiAl), was synthesized via co-precipitation technique and employed for the adsorptive removal of two anionic dyes, Eriochrome Black T (EBT) and Methyl Orange (MO) from water. The surface functionalities, structure and morphology of the new adsorbent (SF-B-CoNiAl) were evaluated via scanning electron microscope (SEM), Fourier transform infrared spectroscopy (FTIR), X-ray diffraction (XRD) and Brunauer–Emmett–Teller (BET) surface area analysis. The batch experiments indicated that the experimental adsorption capacity of SF-B-CoNiAl was 329.61 and 219.56 mg/g for EBT and MO, respectively. Freundlich isotherm best fitted the experimental data signifying heterogeneous surface with multilayer dyes uptake. The adsorption process of anionic dyes onto SF-B-CoNiAl involves both physisorption and chemisorption. The kinetic data of MO and EBT adsorption by SF-B-CoNiAl were well described by the pseudo-second-order kinetic model. The prepared adsorbent exhibited good recyclability that demonstrates their potential for application in water purification.

Keywords Strontium ferrite-bentonite-CoNiAl · Magnetic composite · Layered double hydroxides · Anionic dyes · Adsorption

1 Introduction

Wastewater discharged from chemical industries has remained one of the most significant sources of environmental pollution. Water pollution caused by the dyeing industry is among the substantial menace to the ecosystem, in addition to its impacts on human health [1–5]. The organic dyes (anionic and cationic dyes) are frequently employed in various chemical industries such as textile, plastics, rubber, leather, food, paper and pulp, cosmetics and their release into the ecosystem [6–9]. The global production of dyes is over 0.7 million ton, while around 100 ton of dyes is discharged annually as effluent into watercourses [10–12]. Due to their carcinogenic nature, the presence of dyes in water even in low concentrations can have adverse environmental impacts. Dyes reduce the penetration of sunlight into the water, change the color of water and affect the photosynthetic reaction that harms the aquatic life [9, 12]. It is, therefore, essential to have an effective, simple and low-cost technique for the removal of dyes from wastewater. Eriochrome Black T (EBT) and Methyl Orange (MO) are examples of azo dyes frequently used in textile industries [13, 14].

Different treatment techniques, not limited to, biological, coagulation, flocculation, filtration, ion-exchange and membrane separation, have been employed to decontamination of dyes-polluted water [15–18]. Most of these traditional methods have their respective demerits and constraints such as low efficiency, complexity, high operational cost and less feasibility for applications on a large scale. Attributed to

✉ Ihsanullah Ihsanullah
ihsankhan@kfupm.edu.sa; engr.ihsan.dir@gmail.com

✉ Mamdouh A. Al-Harthi
mamdouh@kfupm.edu.sa

1 Center of Research Excellence in Nanotechnology, King Fahd University of Petroleum and Minerals, Dhahran 31261, Saudi Arabia

2 Center for Environment and Water, Research Institute, King Fahd University of Petroleum and Minerals, Dhahran 31261, Saudi Arabia

3 Department of Environmental Engineering, College of Engineering, Imam Abdulrahman Bin Faisal University, P.O. Box 1982, Dammam 31451, Saudi Arabia

4 Department of Chemical Engineering, King Fahd University of Petroleum and Minerals, Dhahran 31261, Saudi Arabia

its low operating cost, simple process technique and effectiveness in removing various pollutants from the aqueous medium, adsorption has enticed a significant consideration in water treatment [19, 20]. Researchers are in incessant search to develop novel sustainable, efficient, low-cost and less toxic adsorbents for water purification. A large number of adsorbents have been evaluated in the removal of dyes from wastewater such as activated carbon [21], natural and synthetic zeolite [22, 23], bentonite(B) [24], chitosan [25], layered double hydroxides [5, 26], graphene [27], clay [28], MXenes [29] and fly ash [30].

Layered double hydroxides (LDHs) have been engrossed substantial consideration in recent times owing to their applications in numerous areas including water treatment, supercapacitors catalysis, biomedicine and biosensing [5, 31–41]. The common form of LDHs has the formula: $\left[M^{2+}_{1-x}M^{3+}_{x}(\mathrm{OH})_2\right]\left[A^{n-}_{x/n}\cdot m\mathrm{H_2O}\right]$, in which M^{2+} and M^{3+} are metals with divalent and trivalent ions, x is the molar ratio of trivalent cations, A^{n-} is the anion within the interlayer. Currently, LDHs have grabbed an amassed attention in many applications such as supercapacitors [41], catalysis [33], biomedicine and biosensing [32] and water treatment [31]. In water remediation applications, LDH-based composites have emerged as excellent adsorbents for the uptake of various pollutants from aqueous phase [42, 43]. Likewise, bentonite entails essentially of clay minerals of the smectite (montmorillonite) group and has been widely employed as an efficient low-cost adsorbent for the removal of numerous contaminants from water [44–51]. Strontium ferrite ($SrFe_{12}O_{19}$) nanoparticles were also studied by researchers in the various fields owing to their magnetic characteristics [52–54].

In this work, a new magnetic composite comprising bentonite (B) and strontium ferrite (SF) intercalated into layers CoNiAl was prepared via co-precipitation technique. The intercalation of magnetic nanoparticles with bentonite into the layers of CoNiAl is anticipated to improve the surface characteristics (*i.e.,* surface area, functional groups and heterogeneity) and adsorption performance of the CoNiAl for remediation of various pollutants from the water phase. To the best of our knowledge, this is the first investigation reporting the synthesis of strontium ferrite decorated bentonite-CoNiAl magnetic composite. The prepared SF-B-CoNiAl composite was employed for the adsorptive removal of MO and EBT dyes from water. The adsorbent was characterized by SEM, FTIR, XRD and BET surface area analysis. Experiments were performed to investigate the effect of various process parameters, *i.e.,* initial pH, dye concentration, contact time, and adsorbent dosage was evaluated on the adsorption of anionic dyes onto SF-B-CoNiAl in batch experiments. Adsorption equilibrium data were fitted on three isotherm models, *i.e.,* Langmuir, Freundlich and Temkin isotherms. The kinetic data MO and EBT adsorption by SF-B-CoNiAl were evaluated by using pseudo-first-order and pseudo-second-order kinetic models.

2 Experimental

2.1 Materials

Nickel nitrate hexahydrate ($Ni(NO_3)_2{\cdot}6H_2O$), cobalt nitrate hexahydrate ($Co(NO_3)_2{\cdot}6H_2O$), aluminum nitrate nonahydrate ($Al(NO_3)_3{\cdot}9H_2O$) and strontium ferrite nanopowder were purchased from Sigma-Aldrich (Germany). Bentonite ($\rho \sim 2.5$ g/cm^3) was purchased from BDH Chemicals (UK). Liquid nitrogen (99.998%) was purchased from a local supplier in Dammam, Saudi Arabia. All the chemicals were pure (>98%) and used as acquired. The properties of model dyes, *i.e.,* EBT and MO, are presented in Table 1. The stock solutions were prepared by dissolving 1 g of the dye in 1000 mL of deionized (DI) water. The required dye concentrations (20–100) mg/L were obtained by dilution of the stock solution using DI water.

2.2 Synthesis of SF-B-CoNiAl Magnetic Composite

Initially, 250 mg of strontium ferrite and bentonite (50:50) was ultrasonicated in 80 mL of DI water at 100 amplitude for 30 min. The resultant solution is mixed with a solution prepared by blending of 5.82 g of Ni, 2.91 g of Co and 3.73 g of Al (the precursor salts) at a ratio of 2:1:1 in 50 mL DI water at a controlled pH (10) followed by the addition of 2–3 drops of hydrazine-reducing agent under vigorous stirring. The pH was controlled by adding 1.0 M NaOH and 1.0 M HNO_3 solution using pH meter (C5010, Consort, Belgium). Under constant magnetic stirring, the suspension was refluxed at 90 °C for 24 h, centrifuged (Sigma 2–16 P, Sigma Laborzentrifugen, Germany) at (5000 rpm and 5 min) and cleaned using pure ethanol and DI water to ensure all contaminations are eliminated. The magnetic composite obtained was dried at 90 °C for 24 h in an oven (FDL 115, Binder, UK). Lastly, the composite calcination was performed under a nitrogen environment using a tubular furnace (NAB 8129, Nabertherm, Germany) at 350 °C for 3 h.

2.3 Characterization of SF-B-CoNiAl Magnetic Composite

The synthesized composite was characterized by XRD (Rigaku D/Max-rA rotating anode equipped with Cu Kα radiation, $\lambda = 0.1542$ nm and $2\theta = 2°$ to 70° at a scanning rate of 3°/min, USA), FTIR (6700 Nicolet, Thermo-FTIR spectrometer, 32 scans, resolution of 4 cm^{-1} from 400 to 4500 cm^{-1}, USA), SEM (LYRA3, TESCAN Field Emission SEM, Czech

Table 1 Characteristics of EBT and MO

Dye	Chemical formula	Molecular weight	λ_{max} (nm)	Color index/type
EBT	$C_{20}H_{12}N_3NaO_7S$	461.38	530	14645/Azo dye
MO	$C_{14}H_{14}N_3NaO_3S$	327.33	464	13025/Anionic dye

Republic) and BET (Micromeritics, Tristar II series, USA) surface area analysis.

2.4 Point of Zero Charge Analysis

The point of zero charge (pH_{PZC}) was determined by the method known as salt addition method. Nearly, 0.0200 g of adsorbent was added to 10.0 mL of 0.1 M NaCl in 50-mL plastic tubes. The pH was adjusted using a pH meter (C5010, Consort, Belgium) to 2–12 (± 0.1) via 0.1 M HNO_3 and 0.1 M NaOH. The mixture was agitated for 24 h in a shaker (Orbi shaker BT3000, Benchmark, USA). The final pH was measured and plotted vs initial pH.

2.5 Batch Adsorption Experiments

Adsorption experiments in the batch mode were employed to study the effect of key parameters such as reaction time, initial concentration of dye, initial pH and adsorbent dosage on the adsorption of MO and EBT onto SF-B-CoNiAl. About 0.01 g of magnetic composite in 30 mL of a solution of varying dye concentration (20–200) mg/L was agitated for 10–360 min at 180 rpm at room temperature in 50-mL tubes. The pH was regulated by using HNO_3 and NaOH solutions. At the end of each test, the spent adsorbent was detached from the residual dye solution by using centrifugation at 3500 rpm for 5 min. Spectrophotometer (DR 6000, UV–Vis Hach Lange, UK), set at a wavelength of 464 nm and 530 nm for MO and EBT, respectively, was utilized to quantify the residual concentration of dyes. The adsorption performance was calculated using Eqs. (1, 2).

$$\text{Adsorption capacity} = q_e = \frac{(C_o - C_e)}{W} V \tag{1}$$

$$\text{Percentage removal} = \frac{(C_o - C_e)}{C_o} \times 100 \tag{2}$$

where C_o and C_e represent initial and equilibrium dye concentration (mg/L), respectively, V = volume of dye solution (L), q_e = adsorption capacity at equilibrium (mg/g) and W = mass of adsorbent (g).

2.6 Kinetic Modeling

The kinetic data acquired at various dye concentrations were tailored to the linear forms of two most commonly kinetic models, *i.e.,* pseudo-first order [55, 56] and pseudo-second order [57], as shown in Eq. (3) and (4), respectively;

$$\ln(q_e - q_t) = \ln q_e - k_1 t \tag{3}$$

$$\frac{t}{q_t} = \frac{1}{k_2 q_e^2} + \frac{t}{q_e} \tag{4}$$

where k_1 = pseudo-first-order rate constants (min^{-1}) and k_2 = pseudo-second-order rate constant (g mg^{-1} min^{-1}), while q_e (mg g^{-1}) and q_t represent the quantity of dye adsorbed per unit mass of composites at equilibrium and at time t, respectively. The slope and intercept of linear plots of ln ($q_e - q_t$) vs t and t/q_t vs t were used to calculate the parameters of pseudo-first-order (q_e and k_1) and pseudo-second-order (q_e and k_2) kinetic models.

2.7 Isotherm Models

To explore the mechanism of adsorption of the dye molecules onto SF-B-CoNiAl composite, equilibrium data were fitted on three isotherm models, *i.e.,* Langmuir [58], Freundlich [59] and Temkin [60] isotherms. The linear equations of these three isotherm models are stated as follows:

$$\text{Langmuir isotherm model}: \frac{C_e}{q_e} = \frac{1}{K_L q_m} + \frac{C_e}{q_m} \tag{5}$$

$$\text{Freundlich isotherm model}: \ln q_e = \frac{1}{n} \ln C_e + \ln K_f \tag{6}$$

$$\text{Temkin isotherm model}: q_e = \left(\frac{RT}{b_T}\right) \ln A_T + \left(\frac{RT}{b}\right) \ln C_e \tag{7}$$

where n and K_f = Freundlich constants, q_m and q_e = maximum and equilibrium adsorption capacity (mg/g), respectively, K_L = Langmuir constant, T = temperature at 298 K, R = universal gas constant (8.314 J/mol/K), b_T = Temkin isotherm constant, A_T = Temkin isotherm equilibrium binding constant (L/g).

The slope and intercept of linear plots of C_e/q_e versus C_e, $\ln q_e$ versus $\ln C_e$ and q_e versus $\ln C_e$ were used to calculate parameters of Langmuir (q_m and K_L), Freundlich (n and K_F) and Temkin (b_T and A_T), respectively.

2.8 Reusability Performance

The adsorption/desorption experiments were executed to examine the reusability performance of the prepared adsor-

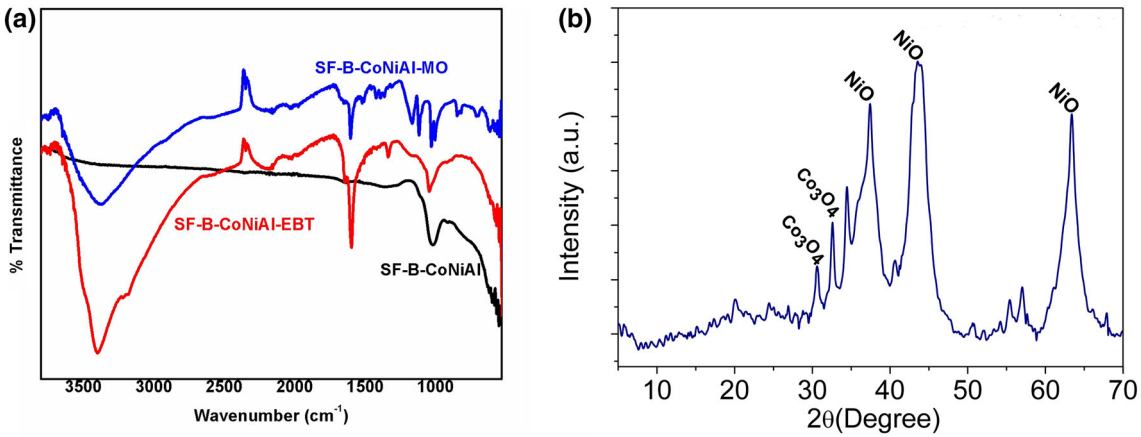

Fig. 1 **a** FTIR spectra of SF-B-CoNiAl before and after adsorption of dyes; **b** XRD patterns of SF-B-CoNiAl

bent. NaOH solution of 0.01 mol/L was used as a regenerating agent. For desorption experiment, MO and EBT-loaded adsorbents (50 mg) were added into the Erlenmeyer flasks comprising of 100 mL solution of regenerating agent. The suspension was briskly agitated on a temperature-controlled shaker for 4 h at 275 rpm and centrifuged to obtain the final solution. After the desorption process, the concentration of MO and EBT was determined using (DR 6000, UV–Vis Hach Lange, UK). The adsorbents were then splashed with distilled water, and restored adsorbents were recycled for four cycles. The removal percentage was determined using Eq. 2.

3 Results and Discussion

3.1 Characterization of SF-B-CoNiAl Magnetic Composite

3.1.1 FTIR and XRD Analysis

Figure 1a, b displays the FTIR spectra and XRD pattern of SF-B-CoNiAl magnetic composite. FTIR spectra of SF-B-CoNiAl show the broadband at 3450–3650 cm^{-1} that corresponds to the OH stretching vibrations. The weak band at 1649 cm^{-1} is assigned to H–O–H bending vibration. The broad peak at 1376 cm^{-1} is associated with the symmetric stretching band of interlayer NO_3 ions. The strong, sharp peak observed at 1029 cm^{-1} is attributed to Si–O and Si–O–Si stretching vibrations. The peaks appeared at 550–650 cm^{-1} are attributed with mixed metal oxides (MMO) that revealed the interaction of SF with CoNiAl during calcination. The FTIR spectrum exhibits all the characteristics peak of bentonite, CoNiAl and SF, indicating that the surface of the composite is abundant with various oxygen functionalities (OH, NO_3, Si–O, Si–O–Si and MMO). These functionalities act as active binding sites and play a vital role in the dyes sorption performance of the composite. After adsorption of dyes, the broad peaks at 3450–3650 cm^{-1} and 1649 cm^{-1} correspond to hydroxyl groups indicating the involvement of –OH groups in the dyes adsorption process. Likewise, the intensity and wave number Si–O and Si–O–Si stretching vibration at 1029 cm^{-1} in SF-B-CoNiAl are shifted after adsorption of both dyes.

The XRD pattern of SF-B-CoNiAl (Fig. 1b) showed almost all characteristic peaks, indicating that the composite is stable after calcination at 500 °C. The weak peaks observed between 20° and 30° represent the SiO_2 amorphous characteristics. The peaks at 25.4°, 53.4° and 59° are assigned to $Sr_2Fe_2O_4$ [61]. The XRD pattern indicated the formation of mixed metal oxides (MMO) at peaks (34.38°, 37.36°, 43.49°, 63.34°) that are associated with NiO, Co_3O_4 and NiO/Co_3O_4 [40, 62, 63]. The basal plane spacing of these peaks is obtained as 2.60, 2.4, 2.07, 1.46, respectively.

3.1.2 Surface Morphology and BET Analysis

Figure 2 shows the SEM images of SF-B-CoNiAl magnetic composite at different magnifications. The magnetic composite exhibits highly rough and porous surface morphology with tiny particles distributed in the entire surface. This is attributed to the presence of porous bentonite layers and strontium ferrite nanoparticles that result in microstructure surface morphology of composite. The high-magnification image of SF-B-CoNiAl (Fig. 2) further confirms that the strontium ferrite nanoparticles are homogenously decorated on the surface of bentonite-CoNiAl, indicating excellent intercalation and improved structure characteristics. Moreover, the SEM images after adsorption of MO and EBT (Fig. 2) indicate the complete transformation of the porous, rough surface into smooth and homogenous morphology.

The BET specific surface area and pore size of SF-B-CoNiAl composite were analyzed using an adsorp-

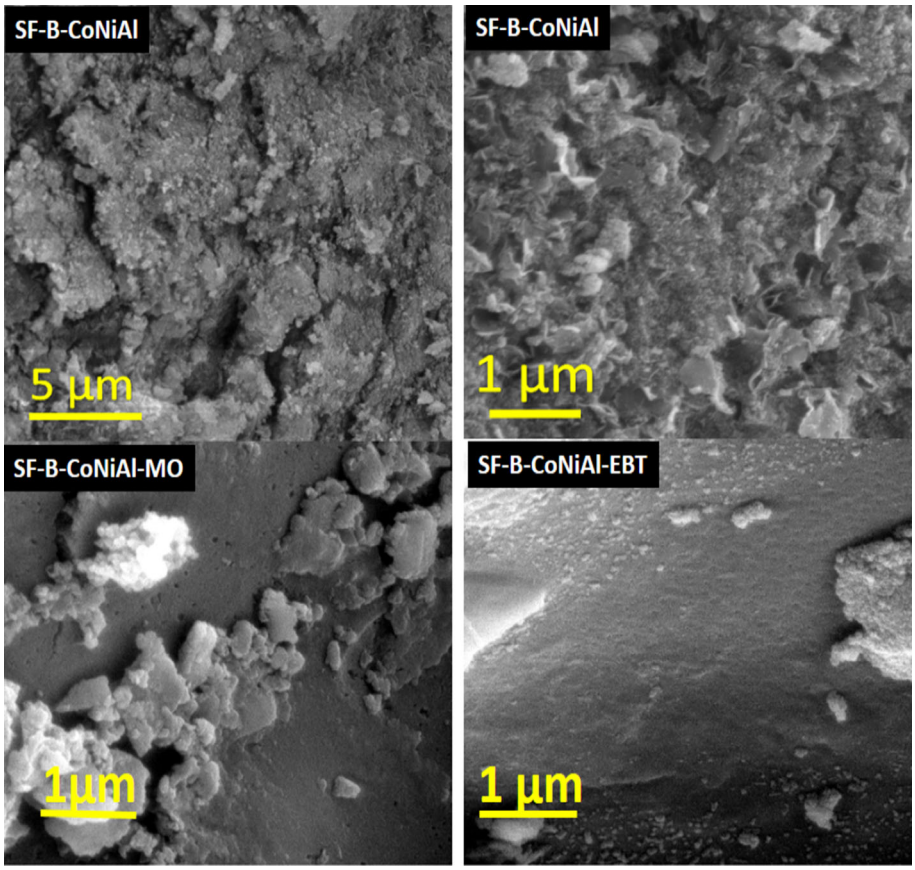

Fig. 2 SEM images of SF-B-CoNiAl at different magnifications before and adsorption of dyes

tion/desorption isotherm in N_2 environment. As presented in Fig. 3, the isotherm at 0.05–1.0 P/P_0 indicates an H3-type hysteresis loop which depicts a type IV isotherm. The BET specific surface area for the SF-B-CoNiAl was 206.23 m^2/g that was higher than many adsorbents reported in the literature [8, 47, 64]. This demonstrates that the SF-B-CoNiAl composite exhibits mesoporous surface characteristics with a comparatively high surface area.

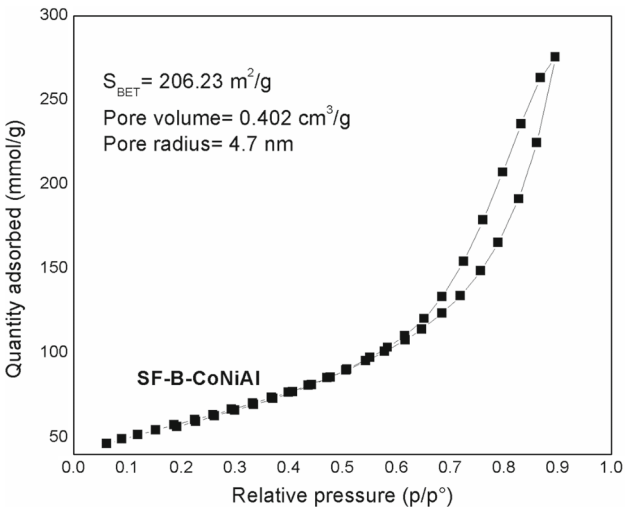

Fig. 3 N_2 adsorption–desorption isotherm of SF-B-CoNiAl

3.2 Effect of Adsorption Parameters

3.2.1 Effect of Initial pH

Solution pH is a crucial parameter that influences removal performance of dyes due to its impact on the adsorbent's surface charge, pollutants ionization degree, active sites functional groups dissociation and the dye molecule structure [3]. The pH impact on the SF-B-CoNiAl adsorptive performance was studied at room temperature in the pH range of 2–10 with 30 mg/L concentration of dye (EBT and MO), an adsorbent dosage of 10 mg, contact time 180 min and shaking at 180 rpm. The results are shown in Fig. 4a. It was observed that the removal of MO increased from 33 to 45% as the pH increased from 2 to 4. At pH > 4, the percentage of MO removal showed a decreasing trend and reduced to 15% removal at pH 10. On the other hand, the removal of EBT reduced significantly from 69 to 22% with an increase in pH from 2 to 4. Further increase in pH value to 10 resulted in a slight change in the removal of EBT. This behavior attributed to the interaction between adsorbent and dye molecules at different pHs and can be explained by point of zero charge (pH_{PZC}) of the adsorbent. Figure 4b shows the pH_{PZC} of

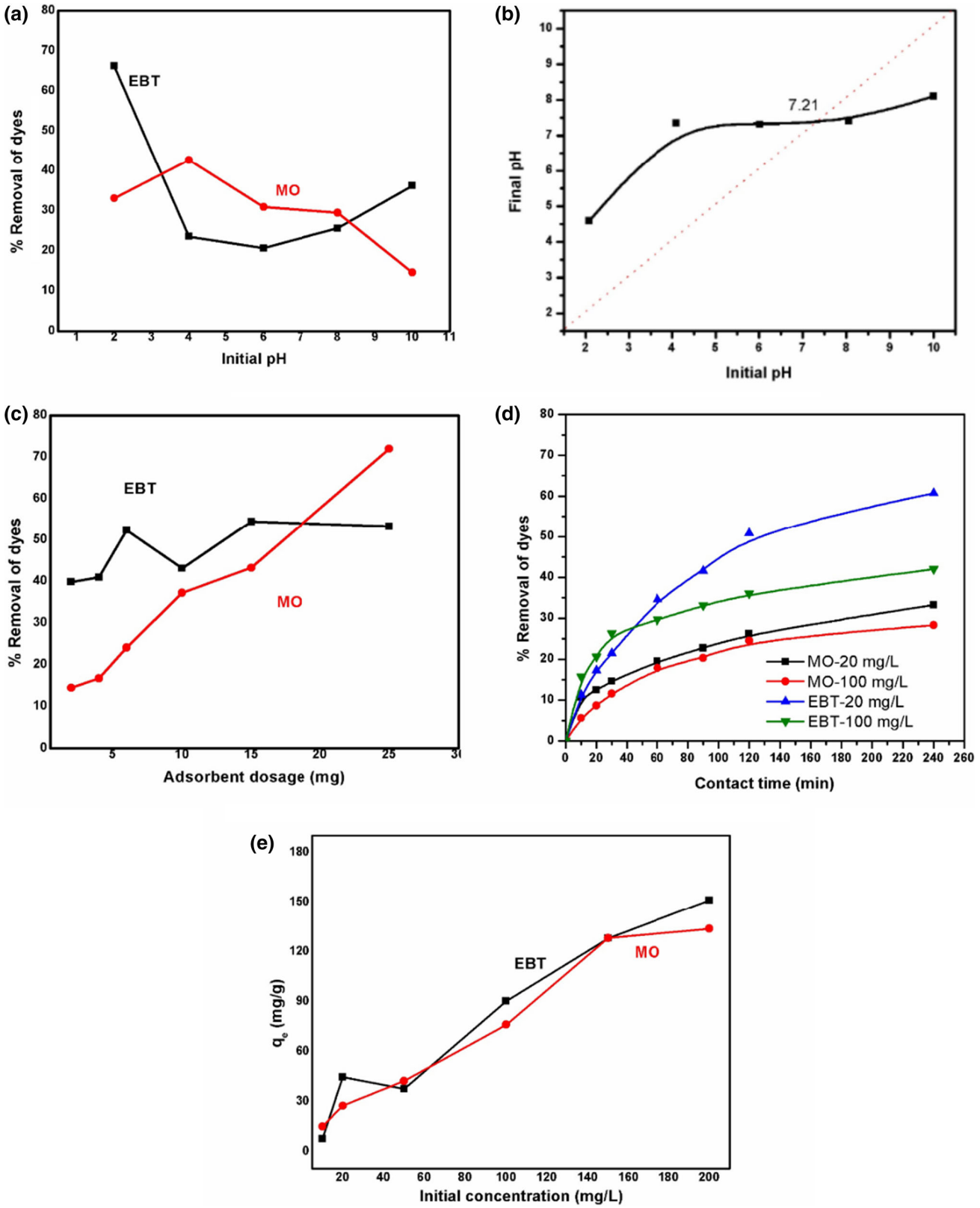

Fig. 4 **a** Effect of initial pH on the removal of MO and EBT (C_0 = 20 mg/L; T = 298 K; dosage = 10 mg); **b** point of zero charge of SF-B-CoNiAl; **c** effect of adsorbent dosage on MO & EBT removal (C_0 = 20 mg/L; T = 298 K; pH = 4 (MO) and 2 (EBT)); **d** effect of contact time on MO & EBT removal (C_0 = 20 mg/L; T = 298 K; dosage = 10 mg, pH = 4 (MO) and 2 (EBT)); **e** effect of initial concentration of MO & EBT on the adsorption capacity (time = 180 min, T = 298 K; dosage = 10 mg, pH = 4 (MO) and 2 (EBT))

SF-B-CoNiAl composite estimated using pH drift method is 7.21. At $pH < pH_{PZC}$ (*i.e.,* pH 2–4), the surface of the SF-B-CoNiAl was positively charged and strong interactions exist between the adsorbent surface and anionic dyes (MO and EBT) via electrostatic attractions. When the dye solution pH was raised, the interaction of adsorbent and adsorbate weakened due to reduction of positively charged sites. Moreover, the lower removal of MO and EBT at $pH > pH_{PZC}$, (higher pH values) is ascribed to the electrostatic repulsion between the dye molecules and negatively charged SF-B-CoNiAl surface. Other different materials employed for anionic dyes uptake exhibited similar behavior [36, 65]. The SF-B-CoNiAl composite showed maximum removal of EBT and MO at pH 2 and pH 4, and these values were selected for later adsorption experiments.

3.2.2 Effect of Adsorbent Dosage

It is well known that the number of accessible active adsorption sites can considerably affect the efficiency of the adsorption process. Therefore, the effect of SF-B-CoNiAl composite dosage (2–25) mg on the adsorptive removal of dyes (EBT and MO) has been investigated at 20 mg/L of dye concentration, the contact time of 180 min and pH 4 (for MO) and 2 (EBT), respectively. As depicted in Fig. 4c, both dyes (MO and EBT) showed a sharp increase in removal as the dosage increases from 0 to 10 mg, respectively. This is due to the increased number of the active adsorption sites with the increase in magnetic composite dosage resulting in higher adsorption of dye. Further increase in dosage from 12 to 25 mg showed a slight or gradual increase in R for EBT and MO, respectively. The maximum removal of 75.85% and 69.25% for EBT and MO, respectively, was obtained at dosage 25 mg. Based on dosage results, 10 mg was selected for equilibrium and kinetic study experiments.

3.2.3 Effect of Contact Time

Under initial dye concentrations of 20 and 100 mg/L, the influence of adsorption period was evaluated at pH 2 and pH 4 for EBT and MO, respectively, with an adsorbent dosage of 10 mg at varied contact time from 0 to 360 min. The results presented in Fig. 4d indicate that the removal of both dyes increased linearly with an increase in contact time from 0 to 60 min. Beyond 60-min gradual change in the removal trends of both dyes is noticeable. The percentage removal values of (33 and 25%) and (69 and 40%) were obtained for MO and EBT after 240 min by SF-B-CoNiAl at 20 and 100 mg/L initial concentrations, respectively. The swift SF-B-CoNiAl adsorptive performances tailed by slow adsorption could be allied with the memory effect of CoNiAl along with higher attractive behaviors between active sites surface functional groups and the dyes molecules. A contact time of 180 min was selected and used in the subsequent experiments.

3.2.4 Effect of Initial Concentration

The initial dye concentration in solution has a substantial effect on the adsorption process, as it linked to the number of dye molecules and the accessible active sites on the surface of the adsorbent [66]. The effect of dye concentration on the sorption performance of SF-B-CoNiAl is displayed in Fig. 4e. Experiments were conducted at concentration ranging from 10 to 200 mg/L, at pH 2 (for EBT) and 4 (for MO), an adsorbent dosage of 10 mg and contact time of 180 min. As shown in Fig. 4e, there is a substantial improvement in adsorption capacity of magnetic adsorbent with the increase in the initial concentration of both dyes. For instance, the adsorption capacity of EBT onto SF-B-CoNiAl increased linearly when the initial EBT concentration was increased from 10 mg/L to 200 mg/L. Likewise, the adsorption of MO on the SF-B-CoNiAl showed a sharp increase up to an initial concentration of 150 mg/L and then no change was observed with further increase in MO concentration to 200 mg/L. The maximum adsorption capacities for magnetic composite achieved at an initial concentration of 200 mg/L EBT and MO were 310.25 and 135.23 mg/g, respectively. The higher adsorption capacity of EBT compared to MO dye was due to the strong interaction of EBT with the adsorbent functional groups.

3.3 Adsorption Kinetic Modeling

To estimate the dyes (EBT and MO) adsorption rate on the SF-B-CoNiAl, pseudo-first-order and pseudo-second-order models were used, and their respected linear plots are depicted in Fig. 5. The estimated parameters of the two applied models are given in Table 2. The correlation coefficient (R^2) value at the studied concentration (20 and 100 mg/L) is close to unity for second-order model for both dyes. Moreover, the root-mean-square error (RMSE) of pseudo-second-order model is lower compared to pseudo-first-order model. This suggests that the kinetic data are well described by pseudo-second order ($R^2 > 0.99$) and that chemisorption mechanisms are involved for MO and EBT adsorption onto magnetic composite. Based on the assumption of the model, the adsorption process of MO and EBT dye molecules onto SF-B-CoNiAl magnetic composite is mainly controlled by chemisorption. Previously investigated magnetic adsorbents reported similar findings for remediation of various anionic dyes [67, 68].

3.4 Adsorption Isotherm Modeling

The linear plots of the isotherm models (Langmuir, Freundlich and Temkin) are displayed in Fig. 6. The estimated

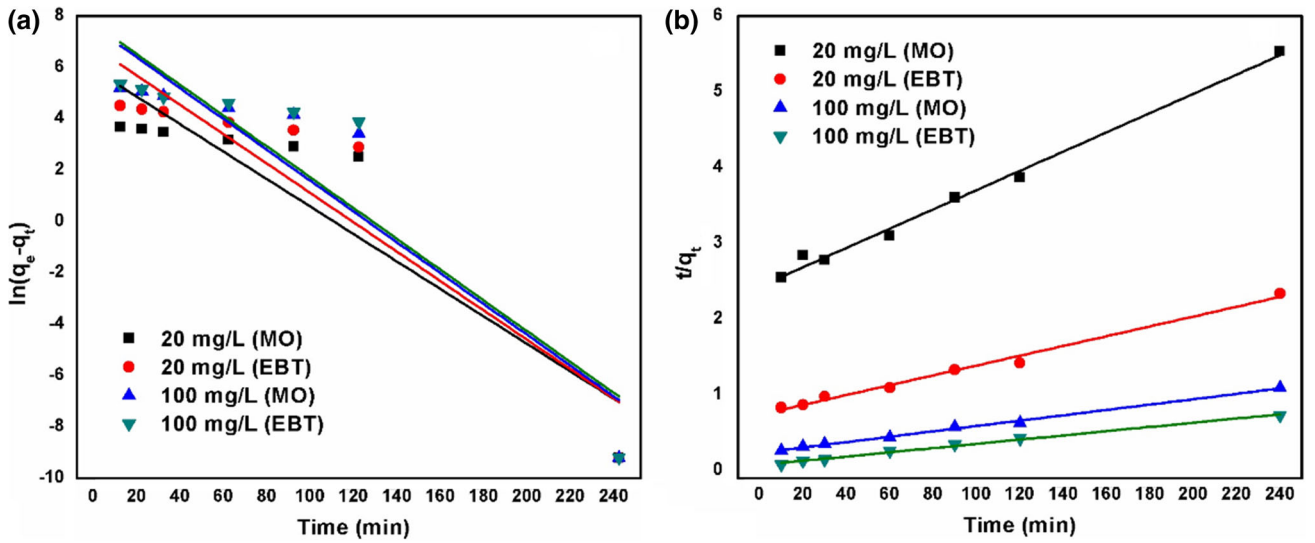

Fig. 5 Linear plots of (**a**) pseudo-first-order and **b** pseudo-second-order model of EBT and MO dye onto SF-B-CoNiAl (Co = 20 and 100 mg/L; pH 2 (EBT) and 4 (MO); dosage = 5 mg; contact time = 0–240 min)

Table 2 Pseudo-first-order and pseudo-second-order kinetic model parameters for adsorption of MO and EBT onto SF-B-CoNiAl composite

Dye	C_o	$q_{e\ (exp)}$	Pseudo-first order			RMSE	Pseudo-second order			RMSE
			q_e	k_1	R^2		q_e	k_2	R^2	
MO	20	43.36	330.29	0.12	0.828	2.140	78.74	6.77	0.992	0.096
	100	219.56	1719.8	0.13	0.850	2.216	285.71	5.19	0.996	0.018
EBT	20	102.56	804.32	0.13	0.845	2.146	153.84	5.81	0.990	0.055
	100	329.61	1939.1	0.13	0.833	2.354	357.14	10.79	0.993	0.019

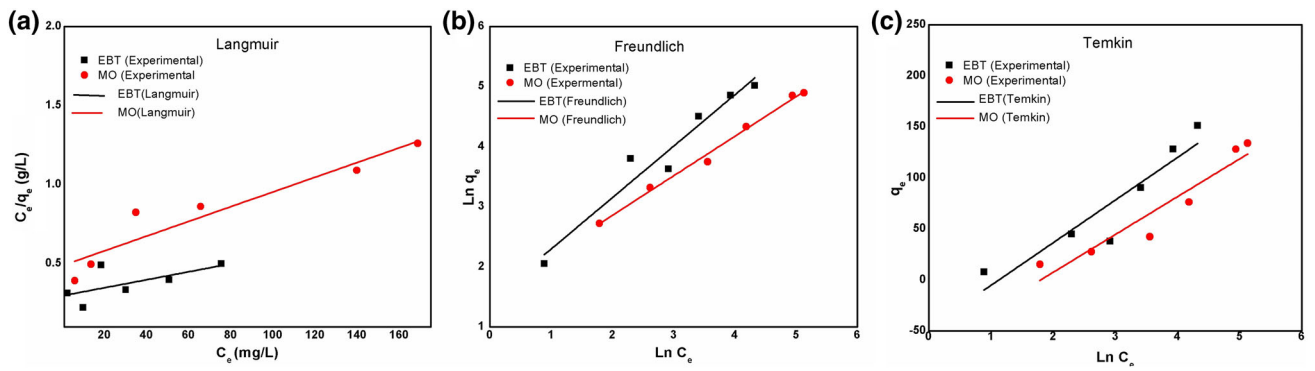

Fig. 6 Linear plots of Langmuir, Freundlich and Temkin isotherm models of EBT and MO dye onto SF-B-CoNiAl (Co = 10–200) mg/L; contact time = 240 min; dosage = 5 mg; pH = 2 (EBT) and 4 (MO)

values of isotherm parameters are summarized in Table 3. The higher values of Freundlich isotherm (R^2 >0.99 (MO) and 0.93 (EBT)) compared to Langmuir (R^2 >0.90 (MO) and 0.41 (EBT)) and Temkin (R^2 >0.88 (MO) and 0.82 (EBT)) demonstrate that the sorption of EBT and MO onto SF-B-CoNiAl is well described by Freundlich isotherm. This indicates the heterogeneous surface nature of composite involving multilayer sorption. The respective maximum adsorption capacity of SF-B- CoNiAl composite calculated from Langmuir isotherm was 214.59 and 395.25 mg/g for MO and EBT. Moreover, the values of Freundlich constant ($0 > 1/n < 1$) signify the favorability of (MO and EBT)-SF-B-CoNiAl adsorption system. The isotherm results demonstrate that the sorption mechanism of dyes involves multilayer adsorption comprising electrostatic attraction and chemical interaction between oxygen functionalities of adsorbent and

Table 3 Adsorption isotherm parameters of MO and EBT onto SF-B-CoNiAl composite at 25 °C

Dye	Langmuir			RMSE	Temkin			RMSE	Freundlich			RMSE
	K_L	q_m	R^2		A_T	b_T	R^2		K_f	$1/n$	R^2	
MO	0.009	214.59	0.904	0.09	0.052	38.64	0.888	17.02	4.64	0.65	0.993	0.08
EBT	0.008	395.25	0.415	0.11	0.041	12.19	0.827	23.28	4.22	0.85	0.934	0.27

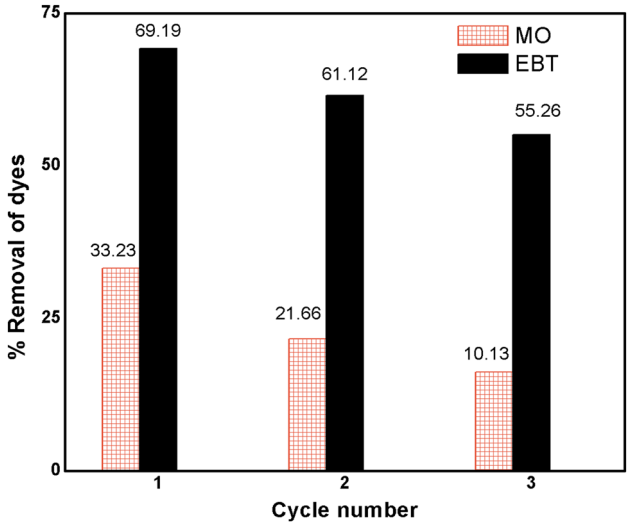

Fig. 7 Regeneration cycles of SF-B-CoNiAl for removal of EBT and MO dye

dye molecules. Similar results have been reported by Rangnath Ravi et al. [67].

3.5 Regeneration Performance

Reusability performance is an essential factor, which assess the suitability of the adsorbent for commercial applications. Desorption of MO and EBT dye from SF-B-CoNiAl was carried out by using 0.01 mol/L NaOH solution. The adsorption efficiency of SF-B-CoNiAl composite for MO and EBT after each cycle is summarized in Fig. 7. The adsorbent displayed relatively stable adsorption performance for EBT in multiple adsorption/desorption cycles. The SF-B-CoNiAl exhibited greater adsorption efficiency of approximately > 50% up to three cycles with a reduction of about 15% in percentage removal after the third cycle, whereas the removal of MO dye was dropped from 33.23 to 10.13% after three cycles. The reduction in SF-B-CoNiAl of dye may be attributed due to the loss of dynamic sites during the whole adsorption–desorption progression. The results showed SF-B-CoNiAl exhibits better reusability performance of EBT as well as MO and suggested as a promising magnetic adsorbent for remediation of anionic pollutants.

3.6 Comparison with Other Adsorbents

The sorption performance of magnetic bentonite-CoNiAl composite for EBT and MO was compared with previously reported adsorbents (Table 4). The results showed the magnetic composite exhibit higher sorption capacity, indicating highly promising and potential to use for the decontamination of anionic dyes. It is important to note that most of the studies reported the maximum adsorption capacities of various adsorbents for the removal of EBT and MO dyes at low pH, *i.e.,* 2–4. This limits the practical applications of these adsorbents for real wastewater. Although some studies reported the successful application of adsorbents for the removal of dyes at pH 6–6.5 that signify the application of such adsorbent in a real situation, the adsorbents surface characteristics should be modified to enhance their adsorption capacity in the pH range of 6 to 8.

4 Conclusions

In summary, a new adsorbent (SF-B-CoNiAl) was synthesized and applied for the technique was the removal of two selected anionic dyes (MO and EBT) from water. The adsorbent showed tremendous performance and removed a significant concentration of both the dyes. The superior performance of the prepared adsorbent can be attributed to the combined characteristics of layered double hydroxide, bentonite and magnetic nature of the strontium ferrite. Freundlich isotherm model best fitted the experimental adsorption data for both dyes signifying a multi-layered adsorption phenomenon. The experimental adsorption capacity of SF-B-CoNiAl was 329.61 and 219.56 mg/g for EBT and MO, respectively. The prepared adsorbent was easily regenerated and employed in three consecutive cycles with a minor loss in adsorption capacity. On this basis, it was concluded that the as-prepared SF-B-CoNiAl is a promising candidate for removing MO and EBT from water.

Table 4 Comparison of adsorption capacity of other adsorbents for removal of EBT and MO

Adsorbent	pH	Time (min)/temp (°C)	Isotherm model/kinetic model	q_m (mg/g)* EBT/MO	References
Eggshells powder (EgP)/SF	2/–	40/45	Langmuir/pseudo-second order	51.18/–	[69]
$NiFe_2O_4$ magnetic nanoparticle	–/6	10/25	Langmuir/pseudo-second order	47.0/–	[70]
Hydrotalcite-like modified bentonite	–/6.5	20/24	Langmuir/pseudo-second order	–/333.3	[71]
Chitosan-saponin-bentonite (CSB) composite film	–/4–5	180/30	Langmuir/pseudo-second order	–/360.9	[72]
Magnetic mesoporous carbon	4	80/25	Langmuir/pseudo-second order	–/110.81	[73]
Diatom-silica xerogel-ceria (DXC)	2	60/Room temperature	Langmuir/pseudo-second order	47.02/–	[74]
SF-B-CoNiAl	2/4	200/25	Freundlich/pseudo-second order	329.61/219.56 (exp)	This study

*q_m = maximum adsorption capacity

Acknowledgements The authors acknowledge the Centre for Nanotechnology (CENT) and the Department of Chemical Engineering, KFUPM, for their support toward the completion of this work.

References

1. Mu'azu, N.D.; Jarrah, N.; Kazeem, T.S.; Zubair, M.; Al-Harthi, M.: Bentonite-layered double hydroxide composite for enhanced aqueous adsorption of Eriochrome Black T. Appl. Clay Sci. **161**, 23–34 (2018). https://doi.org/10.1016/j.clay.2018.04.009
2. Singh, N.B.; Nagpal, G.; Agrawal, S.: Rachna: water purification by using adsorbents: A review. Environ. Technol. Innov. **11**, 187–240 (2018). https://doi.org/10.1016/j.eti.2018.05.006
3. Zubair, M.; Daud, M.; McKay, G.; Shehzad, F.; Al-Harthi, M.A.: Recent progress in layered double hydroxides (LDH)-containing hybrids as adsorbents for water remediation. Appl. Clay Sci. **143**, 279–292 (2017). https://doi.org/10.1016/j.clay.2017.04.002
4. Zubair, M.; Jarrah, N.; Manzar, M.S.; Al-Harthi, M.; Daud, M.; Mu'azu, N.D.; Haladu, S.A.: Adsorption of eriochrome black T from aqueous phase on MgAl-, CoAl- and NiFe- calcined layered double hydroxides: kinetic, equilibrium and thermodynamic studies. J. Mol. Liq. **230**, 344–352 (2017). https://doi.org/10.1016/j.molliq.2017.01.031
5. Zubair, M.; Jarrah, N.; Ihsanullah, K.A.; Manzar, M.S.; Kazeem, T.S.; Al-Harthi, M.A.: Starch-NiFe-layered double hydroxide composites: efficient removal of methyl orange from aqueous phase. J. Mol. Liq. **249**, 254–264 (2018). https://doi.org/10.1016/j.molliq.2017.11.022
6. Monsef, R.; Ghiyasiyan-Arani, M.; Salavati-Niasari, M.: Utilizing of neodymium vanadate nanoparticles as an efficient catalyst to boost the photocatalytic water purification. J. Environ. Manag. **230**, 266–281 (2019). https://doi.org/10.1016/j.jenvman.2018.09.080
7. Sahoo, J.K.; Konar, M.; Rath, J.; Kumar, D.; Sahoo, H.: Magnetic hydroxyapatite nanocomposite: Impact on eriochrome black-T removal and antibacterial activity. J. Mol. Liq. **294**, 111596 (2019). https://doi.org/10.1016/j.molliq.2019.111596
8. Li, X.; Nie, X.-J.; Zhu, Y.-N.; Ye, W.-C.; Jiang, Y.-L.; Su, S.-L.; Yan, B.-T.: Adsorption behaviour of Eriochrome Black T from water onto a cross-linked β-cyclodextrin polymer. Colloids Surf. Physicochem. Eng. Aspects **578**, 123582 (2019). https://doi.org/10.1016/j.colsurfa.2019.123582
9. Jadhav, S.A.; Garud, H.B.; Patil, A.H.; Patil, G.D.; Patil, C.R.; Dongale, T.D.; Patil, P.S.: Recent advancements in silica nanoparticles based technologies for removal of dyes from water. Colloid Interface Sci. Commun. **30**, 100181 (2019). https://doi.org/10.1016/j.colcom.2019.100181
10. Akhouairi, S.; Ouachtak, H.; Addi, A.A.; Jada, A.; Douch, J.: Natural sawdust as adsorbent for the Eriochrome Black T dye removal from aqueous solution. Water Air Soil Pollut. **230**, 181 (2019). https://doi.org/10.1007/s11270-019-4234-6
11. Manzar, M.S.; Waheed, A.; Qazi, I.W.; Blaisi, N.I.; Ullah, N.: Synthesis of a novel epibromohydrin modified crosslinked polyamine resin for highly efficient removal of methyl orange and eriochrome black T. J. Taiwan Inst. Chem. Eng. **97**, 424–432 (2019). https://doi.org/10.1016/j.jtice.2019.01.027
12. Sarker, M.; Shin, S.; Jeong, J.H.; Jhung, S.H.: Mesoporous metal-organic framework PCN-222(Fe): promising adsorbent for removal of big anionic and cationic dyes from water. Chem. Eng. J. **371**, 252–259 (2019). https://doi.org/10.1016/j.cej.2019.04.039
13. Peng, S.; Mao, T.; Zheng, C.; Wu, X.; Wei, Y.; Zeng, Z.; Xiao, R.; Sun, Y.: Polyhydroxyl gemini surfactant-modified montmorillonite for efficient removal of methyl orange. Colloids Surf. Physicochem. Eng. Aspects **578**, 123602 (2019). https://doi.org/10.1016/j.colsurfa.2019.123602
14. Kassem, H.H.; Fahmi, A.R.; Amer, W.A.; Ibrahim, M.N.: Removal of Eriochrom Black T from aqueous solution using Al_2O_3 surface: linear and non-linear isotherm models, error analysis and thermodynamic studies. Mater. Today Proc. **23**, 159 (2019). https://doi.org/10.1016/j.matpr.2019.09.196
15. Das, C.; Rungta, M.; Arya, G.; DasGupta, S.; De, S.: Removal of dyes and their mixtures from aqueous solution using liquid emulsion membrane. J. Hazard. Mater. **159**, 365–371 (2008). https://doi.org/10.1016/j.jhazmat.2008.02.027
16. Zahrim, A.Y.; Hilal, N.: Treatment of highly concentrated dye solution by coagulation/flocculation-sand filtration and nanofiltration. Water Resour. Ind. **3**, 23–34 (2013). https://doi.org/10.1016/j.wri.2013.06.001
17. Papić, S.; Koprivanac, N.; Lončarić Božić, A.; Meteš, A.: Removal of some reactive dyes from synthetic wastewater by combined Al(III) coagulation/carbon adsorption process. Dyes Pigm. **62**, 291–298 (2004). https://doi.org/10.1016/S0143-7208(03)00148-7
18. Pandey, A.; Singh, P.; Iyengar, L.: Bacterial decolorization and degradation of azo dyes. Int. Biodeterior. Biodegrad. **59**, 73–84 (2007). https://doi.org/10.1016/j.ibiod.2006.08.006
19. Ihsanullah, I.; Sajid, M.; Kabeer, M.; Shemsi, A.M.; Atieh, M.A.: First investigations on the removal of tungsten species from water using multi-walled carbon nanotubes. Water Air Soil Pollut. **231**, 119 (2020). https://doi.org/10.1007/s11270-020-04485-2
20. Ihsanullah, A.A.; Al-Amer, A.M.; Laoui, T.; Al-Marri, M.J.; Nasser, M.S.; Khraisheh, M.; Ali, A.M.: Heavy metal removal from aqueous solution by advanced carbon nanotubes: critical review of adsorption applications. Separ. Purif. Technol. **157**, 141–161 (2016). https://doi.org/10.1016/j.seppur.2015.11.039

21. Murray, A.; Örmeci, B.: Competitive effects of humic acid and wastewater on adsorption of methylene blue dye by activated carbon and non-imprinted polymers. J. Environ. Sci. **6**, 310–317 (2017). https://doi.org/10.1016/j.jes.2017.04.029
22. Mthombeni, N.H.; Mbakop, S.; Ray, S.C.; Leswifi, T.; Ochieng, A.; Onyango, M.S.: Highly efficient removal of chromium (VI) through adsorption and reduction: a column dynamic study using magnetized natural zeolite-polypyrrole composite. J. Environ. Chem. Eng. **6**, 4008–4017 (2018). https://doi.org/10.1016/j.jece.2018.05.038
23. Czarna, D.; Baran, P.; Kunecki, P.; Panek, R.; Żmuda, R.; Wdowin, M.: Synthetic zeolites as potential sorbents of mercury from wastewater occurring during wet FGD processes of flue gas. J. Clean. Prod. **172**, 2636–2645 (2016). https://doi.org/10.1016/j.jclepro.2017.11.147
24. Bulut, E.; Özacar, M.; Şengil, I.A.: Equilibrium and kinetic data and process design for adsorption of Congo Red onto bentonite. J. Hazard. Mater. **154**, 613–622 (2008). https://doi.org/10.1016/j.jhazmat.2007.10.071
25. Yuvaraja, G.; Chen, D.-Y.; Pathak, J.L.; Long, J.; Venkata Subbaiah, M.; Wen, J.-C.; Pan, C.-L.: Preparation of novel aminated chitosan schiff's base derivative for the removal of methyl orange dye from aqueous environment and its biological applications. Int. J. Biol. Macromol. (2019). https://doi.org/10.1016/j.ijbiomac.2019.09.236
26. Blaisi, N.I.; Zubair, M.; Ihsanullah, A.S.; Kazeem, T.S.; Manzar, M.S.; Al-Kutti, W.; Al Harthi, M.A.: Date palm ash-MgAl-layered double hydroxide composite: sustainable adsorbent for effective removal of methyl orange and eriochrome black-T from aqueous phase. Environ. Sci. Pollut. Res. **25**, 34319–34331 (2018). https://doi.org/10.1007/s11356-018-3367-2
27. Baig, N.; Ihsanullah, S.M.; Saleh, T.A.: Graphene-based adsorbents for the removal of toxic organic pollutants: a review. J. Environ. Manag. **244**, 370–382 (2019). https://doi.org/10.1016/j.jenvman.2019.05.047
28. Akar, S.T.; Uysal, R.: Untreated clay with high adsorption capacity for effective removal of C.I. Acid Red 88 from aqueous solutions: batch and dynamic flow mode studies. Chem. Eng. J. **162**, 591–598 (2010). https://doi.org/10.1016/j.cej.2010.06.001
29. Ihsanullah, I.: MXenes (two-dimensional metal carbides) as emerging nanomaterials for water purification: progress, challenges and prospects. Chem. Eng. J. **388**, 124340 (2020). https://doi.org/10.1016/j.cej.2020.124340
30. Wang, N.; Zhao, Q.; Xu, H.; Niu, W.; Ma, L.; Lan, D.; Hao, L.: Adsorptive treatment of coking wastewater using raw coal fly ash: adsorption kinetic, thermodynamics and regeneration by Fenton process. Chemosphere **210**, 624–632 (2018). https://doi.org/10.1016/J.CHEMOSPHERE.2018.07.073
31. Daud, M.; Kamal, M.S.; Shehzad, F.; Al-Harthi, M.A.: Graphene/layered double hydroxides nanocomposites: a review of recent progress in synthesis and applications. Carbon **104**, 241–252 (2016). https://doi.org/10.1016/j.carbon.2016.03.057
32. Grosu, E.F.: Layered double hydroxides nanomaterials in biomedicine and (bio) sensing design. Biomed. J. Sci. Tech. Res. **2**, 2–7 (2018). https://doi.org/10.26717/BJSTR.2018.02.000786
33. Xu, Z.P.; Zhang, J.; Adebajo, M.O.; Zhang, H.; Zhou, C.: Catalytic applications of layered double hydroxides and derivatives. Appl. Clay Sci. **53**, 139–150 (2011). https://doi.org/10.1016/j.clay.2011.02.007
34. Wang, Q.; Ohare, D.: Recent advances in the synthesis and application of layered double hydroxide (LDH) nanosheets. Chem. Rev. **112**, 4124–4155 (2012). https://doi.org/10.1021/cr200434v
35. Newman, S.P.; Jones, W.: Synthesis, characterization and applications of layered double hydroxides containing organic guests. New J. Chem. **22**, 105–115 (1998). https://doi.org/10.1039/a708319j
36. Guo, X.; Yin, P.; Yang, H.: Superb adsorption of organic dyes from aqueous solution on hierarchically porous composites constructed by ZnAl-LDH/Al(OH)3 nanosheets. Microporous Mesoporous Mater. **259**, 123–133 (2018). https://doi.org/10.1016/j.micromeso.2017.10.003
37. Chen, L.; Li, C.; Wei, Y.; Zhou, G.; Pan, A.; Wei, W.; Huang, B.: Hollow LDH nanowires as excellent adsorbents for organic dye. J. Alloy. Compd. **687**, 499–505 (2016). https://doi.org/10.1016/j.jallcom.2016.05.344
38. El, K.; Horax, B.; Kalnina, D.; Oukani, E.; Anouar, A.: Effect of morphological properties of layered double hydroxides on adsorption of azo dye methyl orange: a comparative study. Appl. Clay Sci. **140**, 124–131 (2017). https://doi.org/10.1016/j.clay.2017.02.010
39. Cao, Y.; Li, G.; Li, X.: Graphene/layered double hydroxide nanocomposite: properties, synthesis, and applications. Chem. Eng. J. **292**, 207–223 (2016). https://doi.org/10.1016/j.cej.2016.01.114
40. Ramakrishna, K.R.; Viraraghavan, T.: Dye removal using low cost adsorbents. Water Sci. Technol. **36**, 189–196 (1997). https://doi.org/10.1016/s0273-1223(97)00387-9
41. He, F.; Hu, Z.; Liu, K.; Guo, H.; Zhang, S.; Liu, H.; Xie, Q.: Facile fabrication of GNS/NiCoAl-LDH composite as an advanced electrode material for high-performance supercapacitors. J. Solid State Electrochem. **19**, 607–617 (2014). https://doi.org/10.1007/s10008-014-2644-3
42. Shou, J.; Jiang, C.; Wang, F.; Qiu, M.; Xu, Q.: Fabrication of Fe3O4/MgAl-layered double hydroxide magnetic composites for the effective decontamination of Co(II) from synthetic wastewater. J. Mol. Liq. **207**, 216–223 (2015). https://doi.org/10.1016/j.molliq.2015.03.047
43. Zhang, X.; Wang, J.; Li, R.; Dai, Q.; Gao, R.; Liu, Q.; Zhang, M.: Preparation of Fe3O4@C@ layered double hydroxide composite for magnetic separation of uranium. Ind. Eng. Chem. Res. **52**, 10152–10159 (2013). https://doi.org/10.1021/ie3024438
44. Pandey, S.: A comprehensive review on recent developments in bentonite-based materials used as adsorbents for wastewater treatment. J. Mol. Liq. **241**, 1091–1113 (2017). https://doi.org/10.1016/j.molliq.2017.06.115
45. Alexander, J.A.; Ahmad, Z.M.A.; Surajudeen, A.; Aliyu, E.-N.U.; Omeiza, A.U.: Surface modification of low-cost bentonite adsorbents—a review. Part. Sci. Technol. **37**, 538–549 (2019). https://doi.org/10.1080/02726351.2018.1438548
46. Pourshadlou, S.; Mobasherpour, I.; Majidian, H.; Salahi, E.; Shirani, B.F.; Mei, C.-T.; Ebrahimi, M.: Adsorption system for Mg^{2+} removal from aqueous solutions using bentonite/γ-alumina nanocomposite. J. Colloid Interface Sci. **568**, 245–254 (2020). https://doi.org/10.1016/j.jcis.2020.01.036
47. Lin, J.; He, S.; Zhan, Y.; Zhang, H.: Evaluation of phosphate adsorption on zirconium/magnesium-modified bentonite. Environ. Technol. **41**, 586–602 (2020). https://doi.org/10.1080/09593330.2018.1505966
48. Koyuncu, H.: Adsorption kinetics of 3-hydroxybenzaldehyde on native and activated bentonite. Appl. Clay Sci. **38**, 279–287 (2008). https://doi.org/10.1016/j.clay.2007.03.010
49. Doulia, D.; Leodopoulos, C.; Gimouhopoulos, K.; Rigas, F.: Adsorption of humic acid on acid-activated Greek bentonite. J. Colloid Interface Sci. **340**, 131–141 (2009). https://doi.org/10.1016/j.jcis.2009.07.028
50. Ahmaruzzaman, M.: Adsorption of phenolic compounds on low-cost adsorbents: a review. Adv. Coll. Interface. Sci. **143**, 48–67 (2008). https://doi.org/10.1016/j.cis.2008.07.002
51. Banat, F.A.; Al-Bashir, B.; Al-Asheh, S.; Hayajneh, O.: Adsorption of phenol by bentonite. Environ. Pollut. **107**, 391–398 (2000). https://doi.org/10.1016/S0269-7491(99)00173-6
52. Zhao, D.; Li, Q.; Ye, Y.; Zhang, C.: Synthesis and characterization of carbon nanotubes decorated with strontium ferrite nanoparti-

cles. Synth. Metals. **160**, 866–870 (2010). https://doi.org/10.1016/j.synthmet.2010.01.036
53. Luo, J.; Shen, P.; Yao, W.; Jiang, C.; Xu, J.: Synthesis, characterization, and microwave absorption properties of reduced graphene oxide/strontium ferrite/polyaniline nanocomposites. Nanoscale Res. Lett. **11**, 141 (2016). https://doi.org/10.1186/s11671-016-1340-x
54. Sahoo, J.K.; Konar, M.; Rath, J.; Kumar, D.; Sahoo, H.: Hexagonal strontium ferrite: cationic dye adsorption and antibacterial activity. Sep. Sci. Technol. **55**, 415–430 (2020). https://doi.org/10.1080/01496395.2019.1577267
55. McKay, G.; McConvey, I.F.: Zur theorie der sogenannten adsorption gelöster stoffe. J. Chem. Tech. Biotech. **31**, 401–408 (1981)
56. Ho, Y.S.; Mckay, G.: Kinetic models for the sorption of dye from aqueous solution by wood. Process Saf. Environ. Prot. **76**, 183–191 (1998). https://doi.org/10.1205/095758298529326
57. Ho, Y.S.; McKay, G.: Pseudo-second order model for sorption processes. Process Biochem. **34**, 451–465 (1999). https://doi.org/10.1016/S0032-9592(98)00112-5
58. Langmuir, I.: The constitution and fundamental properties of solids and liquids. J. Am. Chem. Soc. **38**, 2221–2295 (1916). https://doi.org/10.1021/ja02268a002
59. Freundlich, H.M.F.: Uber die adsorption in losungen. Zeitschrift fur Physikalische Chemie (Leipzig). 385–470 (1906)
60. Temkin, M.J.; Pyzhev, V.: Recent modifications to Langmuir isotherms. Acta Physiochim. URSS. **12**, 217–222 (1940)
61. Kaur, P.; Singh, S.; Kumar, V.; Tikoo, K.B.; Chudasama, B.; Kaushik, A.; Singhal, S.: Interesting makeover of strontium hexaferrites for environment remediation from excellent photocatalysts to outstanding adsorbents via inclusion of Mn^{3+} into the lattice. J. Alloy. Compd. **791**, 508–521 (2019). https://doi.org/10.1016/j.jallcom.2019.03.312
62. Clause, O.; Goncalves Coelho, M.; Gazzano, M.; Matteuzzi, D.; Trifirò, F.; Vaccari, A.: Synthesis and thermal reactivity of nickel-containing anionic clays. Appl. Clay Sci. **8**, 169–186 (1993). https://doi.org/10.1016/0169-1317(93)90035-Y
63. Reichle, W.T.: Synthesis of anionic clay minerals (mixed metal hydroxides, hydrotalcite). Solid States Ionics. **22**, 135–141 (1986)
64. Aslam, Z.; Qaiser, M.; Ali, R.; Abbas, A.; Ihsanullah, Z.S.: Al_2O_3/MnO_2/CNTs nanocomposite: Synthesis, characterization and phenol adsorption. Fullerenes Nanotubes Carbon Nanostruct. **27**, 591–600 (2019). https://doi.org/10.1080/1536383X.2019.1622528
65. Zaghouane-Boudiaf, H.; Boutahala, M.; Arab, L.: Removal of methyl orange from aqueous solution by uncalcined and calcined MgNiAl layered double hydroxides (LDHs). Chem. Eng. J. **187**, 142–149 (2012). https://doi.org/10.1016/j.cej.2012.01.112
66. Yagub, M.T.; Sen, T.K.; Afroze, S.; Ang, H.M.: Dye and its removal from aqueous solution by adsorption: a review. Adv. Coll. Interface. Sci. **209**, 172–184 (2014). https://doi.org/10.1016/j.cis.2014.04.002
67. Ravi, R.; Iqbal, S.; Ghosal, A.; Ahmad, S.: Novel mesoporous trimetallic strontium magnesium ferrite (Sr0.3Mg0.7Fe2O4) nanocubes: a selective and recoverable magnetic nanoadsorbent for Congo red. J. Alloys Compd. **791**, 336–347 (2019). https://doi.org/10.1016/j.jallcom.2019.03.305
68. Leiw, M.Y.; Guai, G.H.; Wang, X.; Tse, M.S.; Ng, C.M.; Tan, O.K.: Dark ambient degradation of Bisphenol A and Acid Orange 8 as organic pollutants by perovskite SrFeO3-δ metal oxide. J. Hazard. Mater. **260**, 1–8 (2013). https://doi.org/10.1016/j.jhazmat.2013.04.031
69. Zafar, M.N.; Amjad, M.; Tabassum, M.; Ahmad, I.; Zubair, M.: SrFe2O4 nanoferrites and SrFe2O4/ground eggshell nanocomposites: fast and efficient adsorbents for dyes removal. J. Clean. Prod. **199**, 983–994 (2018). https://doi.org/10.1016/j.jclepro.2018.07.204
70. Moeinpour, F.; Alimoradi, A.; Kazemi, M.: Efficient removal of Eriochrome black-T from aqueous solution using $NiFe_2O_4$ magnetic nanoparticles. J. Environ. Health Sci. Eng. **12**, 112 (2014). https://doi.org/10.1186/s40201-014-0112-8
71. Chen, Y.; Peng, J.; Xiao, H.; Peng, H.; Bu, L.; Pan, Z.; He, Y.; Chen, F.; Wang, X.; Li, S.: Adsorption behavior of hydrotalcite-like modified bentonite for Pb^{2+}, Cu^{2+} and methyl orange removal from water. Appl. Surf. Sci. **420**, 773–781 (2017). https://doi.org/10.1016/j.apsusc.2017.05.138
72. Laysandra, L.; Ondang, I.J.; Ju, Y.H.; Ariandini, B.H.; Mariska, A.; Soetaredjo, F.E.; Putro, J.N.; Santoso, S.P.; Darsono, F.L.; Ismadji, S.: Highly adsorptive chitosan/saponin-bentonite composite film for removal of methyl orange and Cr(VI). Environ. Sci. Pollut. Res. **26**, 5020–5037 (2019). https://doi.org/10.1007/s11356-018-4035-2
73. Chen, R.; Zhai, S.; Lu, W.; Wei, J.; Xu, J.; Lu, A.; Jiang, H.: Facile one-pot solvothermal synthesis of magnetic mesoporous carbon for the efficient adsorption of methyl orange. Environ. Sci. Pollut. Res. (2020). https://doi.org/10.1007/s11356-019-07492-x
74. Sriram, G.; Uthappa, U.T.; Rego, R.M.; Kigga, M.; Kumeria, T.; Jung, H.-Y.; Kurkuri, M.D.: Ceria decorated porous diatom-xerogel as an effective adsorbent for the efficient removal of Eriochrome Black T. Chemosphere **238**, 124692 (2020). https://doi.org/10.1016/j.chemosphere.2019.124692